European Journal of Medicinal Chemistry 87 (2014) 540–551

Contents lists available at ScienceDirect

European Journal of Medicinal Chemistry

journal homepage: http://www.elsevier.com/locate/ejmech

Original article

Design, synthesis and evaluation of multifunctional salphen derivatives for the treatment of Alzheimer's disease

Neng Jiang, Su-Yi Li, Sai-Sai Xie, Zhong-Rui Li, Kelvin D.G. Wang, Xiao-Bing Wang*, Ling-Yi Kong*

State Key Laboratory of Natural Medicines, Department of Natural Medicinal Chemistry, China Pharmaceutical University, 24 Tong Jia Xiang, Nanjing 210009, People's Republic of China

ARTICLE INFO

Article history:
Received 8 July 2014
Received in revised form
28 September 2014
Accepted 1 October 2014
Available online 2 October 2014

Keywords:
Alzheimer's disease
Antioxidant
β-Amyloid aggregation
Metal chelator
Neuroprotection
The blood–brain barrier

ABSTRACT

A series of salphen derivatives (**1**–**26**) have been designed, synthesized, and evaluated as chemical reagents that target and modulate multiple facets of Alzheimer's disease. Most of the compounds exhibit a significant ability to inhibit self-induced and Cu^{2+}-induced β-amyloid ($A\beta_{1-42}$) aggregation, and to function as potential antioxidants and biometal chelators. In particular, the antioxidant activity of compound **2** is 2.6-fold of the trolox value by using the ABTS radical scavenging method, and it also shows a significant ability to inhibit self-induced and Cu^{2+}-induced β-amyloid ($A\beta_{1-42}$) aggregation (70.3%, 20 μM and 85.7%, 50 μM, respectively). Moreover, it is capable of decreasing reactive oxygen species (ROS) induced by Cu^{2+}-Aβ, shows a good neuroprotective effect in human SH-SY5Y neuroblastoma cells and can cross the blood–brain barrier. In addition, compound **2** retains the activities of antioxidant, anti Aβ aggregation and neuroprotection after capturing the metal ions Cu^{2+}, Fe^{3+} and Zn^{2+} (its metal complexes **18**, **22** and **23**). Taken together, these results suggest that compound **2** might be a promising lead compound for AD treatment.

1. Introduction

Alzheimer's disease (AD) is a dreadful neurological illness characterized by a loss of brain function, affecting memory, cognition, and behavior [1,2]. To date there is no treatment for AD and its diagnosis with high accuracy requires a detailed post-mortem examination of the brain [3]. The "amyloid hypothesis" of AD states the brains of AD patients are characterized by the deposition of amyloid plaques whose main component is the amyloid β (Aβ) peptide generated via cleavage of the amyloid precursor protein (APP) by β- and γ-secretases [4–9]. The progressive accumulation of Aβ is accompanied by oxidative stress and inflammation, which leads to neurodegeneration. Therefore, prevention of Aβ aggregation in the brain is currently being considered as a potential therapy for AD.

Aβ shows high affinity for metal ions such as Zn^{2+} and Cu^{2+} which are able to accelerate the formation of Aβ aggregates and neurofibrillary tangles. Metal–Aβ species have been studied to determine their contribution to AD neuropathogenesis [10–19]. Several findings have suggested that two avenues for metal–Aβ species are linked to neurotoxicity: the facilitation of Aβ aggregation and the induction of oxidative stress through ROS generation, leading to neuronal cell death and cognitive impairment. The neurotoxic effects that could be induced by metal–Aβ species may be related to the disruption of membranes leading to apoptosis and/or aggregate accumulation at and around the synapse resulting in weakened cell signaling and neuronal death [10]. The second avenue of neurotoxicity is associated with oxidative stress. When metal ions are surrounded by Aβ species, ROS such as hydrogen peroxide (H_2O_2) and hydroxyl radicals (˙OH) can be generated. Cu(I)–Aβ oligomers have been suggested to contain a highly O_2 reactive Cu(I) center, which may also assist in the formation of ROS [20]. Overall, metal-induced Aβ aggregation and oxidative stress could be attributed to a high degree of neurotoxicity leading to neuronal death and ultimately, cognitive impairment. Thus, the modulation of metal–Aβ interaction and the successful protection of neuronal cells from oxidative damage becomes a promising way to inhibit the Aβ aggregation and thereby reduce the neurotoxicity of Aβ deposits [21].

Resveratrol (trans-3,4,5-trihydroxystilbene), a phytoalexin with a stilbene structure is present in medicinal plants, grape skin,

* Corresponding authors.
E-mail addresses: xbwang@cpu.edu.cn (X.-B. Wang), cpu_lykong@126.com, lykong@cpu.edu.cn (L.-Y. Kong).

http://dx.doi.org/10.1016/j.ejmech.2014.10.004
0223-5234/

peanuts, and red wine. It was shown that resveratrol could counteract Aβ toxicity by its antioxidant properties in cellular models [22], and also could inhibit Aβ aggregation in vitro [23]. ^{18}F-labeled stilbene derivatives have been developed as PET radiotracers for imaging amyloid plagues in the brain, which implies the stilbene structure has a strong affinity to Aβ aggregates [24,25]. (*E*)-N^1,N^1-dimethyl-N^4-(pyridin-2-ylmethylene)benzene-1,4-diamine (**L1**, Fig. 1), can modulate metal-induced Aβ aggregation and ROS production, leading to reduction of metal–Aβ neurotoxicity in living cells [26]. The metal chelator clioquinol (**CQ**) has moved into clinical trials and showed improved cognition. Long-term use is, however, limited by an adverse side effect, subacute myelo-optic neuropathy [27]. Although these metal chelators have an adverse side effect, some studies using these compounds show the involvement of metal ions in AD pathogenesis [28].

Very recently, our group has reported the synthesis of tacrine–coumarin hybrids and (*E*)-*N*-benzylideneaniline derivatives as multi-targeted agents against AD [29–31]. To develop a chemical tool capable of both targeting and modulating the reactivity of multiple AD pathological factors in biological systems, we designed a novel multifunctional ligand (**ML**) with the potential for interaction with Aβ, metal–Aβ, metal chelation, control of ROS generation and antioxidant activity (Fig. 1). For Aβ/metal–Aβ interactions and metal chelation, **ML** was constructed by combining Resveratrol, a known Aβ imaging agent, with **L1**, a molecule previously reported to target and regulate metal–Aβ and **CQ**, a metal chelator (Fig. 1). For enhanced metal binding properties, (N^1E, N^2E)-N^1,N^2-dibenzylidenebenzene-1,2-diamine, along with oxygen donor, was chosen as basic structure of bifunctional small molecules affording a tetradentate ligand for Cu(II) with 1:1 metal-to-ligand stoichiometry. For antioxidant activity, substituents (i.e., phenolic groups, Fig. 1) [32–34] known to have antioxidant capability were integrated into **ML**. We investigated whether salphen derivative complexes, after capturing metal ion like Cu^{2+}, Fe^{3+} and Zn^{2+}, could retain the activities of anti Aβ aggregation, antioxidant, and neuroprotection, and continue to play a role in Alzheimer's disease. Their corresponding metal complexes have been designed to accomplish this.

In this paper, we described the design, synthesis and pharmacological evaluation of a series of salphen derivatives and their metal complexes as multifunctional anti-AD agents. The pharmacological evaluations of these compounds include antioxidant, self-induced and Cu^{2+}-induced Aβ aggregation, ROS induced by Cu^{2+}–Aβ, metal chelation, neuroprotection and the blood–brain barrier.

2. Result and discussion

2.1. Chemistry

The (N^1E,N^2E)-N^1,N^2-dibenzylidenebenzene-1,2-diamine derivatives **1**–**15** were synthesized as previously described [35]. The commercially available 1,2-phenylenediamine derivatives were reacted in ethanol with two equivalents of the respective salicylaldehyde derivatives under reflux condition (Scheme 1). Structures of all synthesized compounds were characterized by comparison with ^{1}H and ^{13}C nuclear magnetic resonance (NMR) spectroscopy data reported in the literature. The salphen metal complexes **16**–**26** were synthesized by reacting the respective salicylaldehyde with the corresponding diamine in the presence of either $FeCl_3 \cdot 6H_2O$, $Cu(OAc)_2 \cdot H_2O$ or $Zn(OAc)_2 \cdot 2H_2O$ under reflux condition (Scheme 1).

The paramagnetism of the iron and copper complexes made a characterization by NMR spectroscopy impossible. However, the coordination of the ligands to iron(III) and copper(II) could be

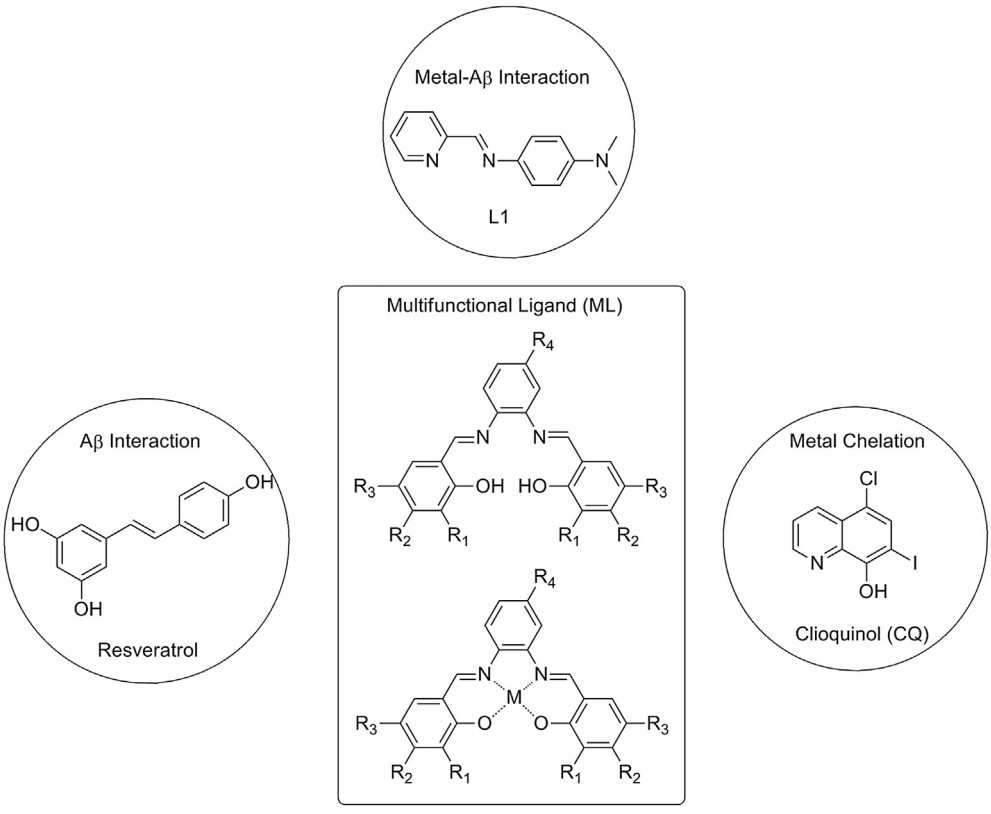

Fig. 1. Combination of the main features of resveratrol, L1 and clioquinol provides molecules with multifunctionality (metal chelation, Aβ interaction, and antioxidant).

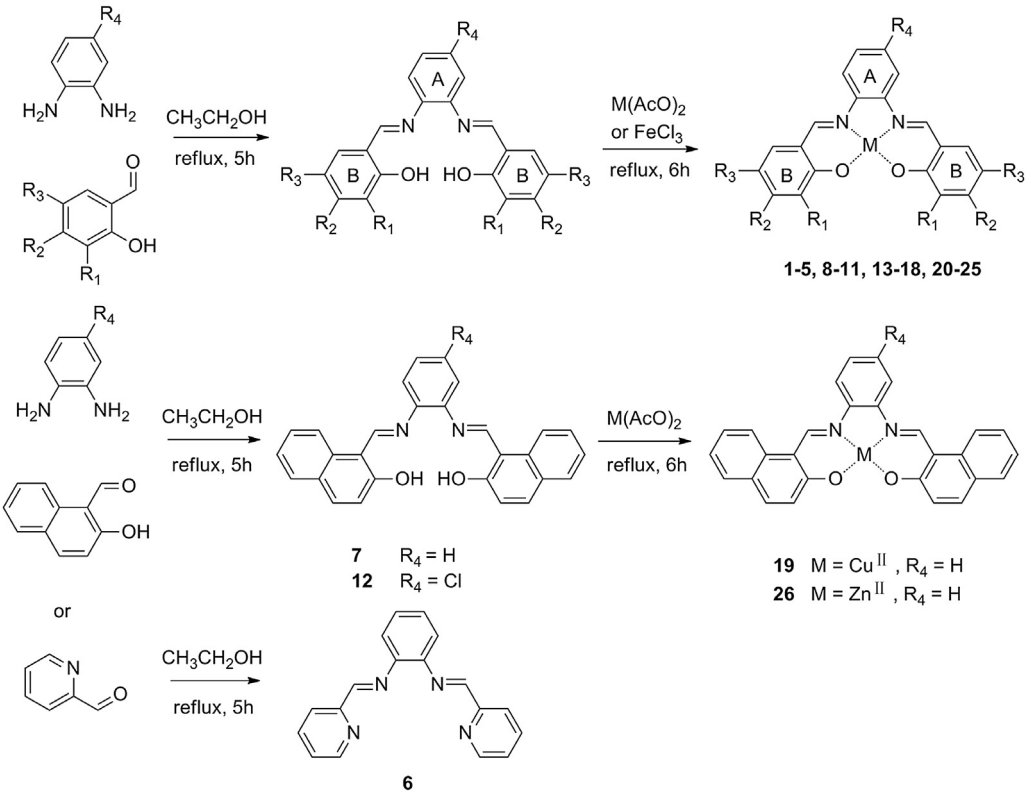

Scheme 1. Structure scheme of salphen derivatives and chemical structure of compounds investigated.

verified by some measurements (IR, Mass and Elemental analyses). In the IR spectra of iron and copper complexes, new bands arise in the region between 600 and 400 cm^{-1} vibration bands of the Fe–N ($\nu \approx 540$ cm^{-1}), the Fe–O ($\nu = 470$ cm^{-1}), Cu–N ($\nu \approx 546$ cm^{-1}), the Cu–O ($\nu = 427$ cm^{-1}) [34]. The others were elucidated by spectroscopic measurements (IR, Mass, ^{1}H NMR and ^{13}C NMR). The IR spectra of titled compounds (**1**–**26**) showed absorption bands of skelton vibrations for benzene rings at 1480–1590 cm^{-1}. The characteristic strong bands appeared for C=N stretching at 1596–1637 cm^{-1}. In the ^{1}H NMR spectra, aromatic protons appeared as set of multiplet in the region δ 5.22–8.54 ppm and CH=N protons resonated as a singlet between δ 8.43 and 9.70 ppm. Moreover, in the ^{13}C NMR spectra, the carbon resonance frequencies of the CH=N was at δ 162.04–175.20 ppm. The aromatic carbons appeared at δ 102.81–164.57 ppm. Finally, the $-OCH_3$ groups appeared at δ 52.64–56.14 ppm.

2.2. Radical-scavenging activity

DPPH (diphenyl-1-picrylhydrazyl) radicals can be used in preliminary screening of compounds capable of scavenging reactive oxygen species, since these nitrogen radicals are much more stable and easier to handle than oxygen free radicals [34]. For comparison purpose, resveratrol was used as reference compound. The IC_{50} values of all tested compounds are summarized in Table 1. From the table, it could be seen that compounds **2**, **11**, **18**, **22** and **23** had much better scavenging activities than resveratrol, while compounds **3**, **4**, **10**, **13**, **14**, **19**, **24** and **25** had similar radical scavenging activities compared to resveratrol. These results indicated that the position of the OH group was critical in determination of scavenging activity. Compounds with a hydroxyl group at the 5 position of the ring B, exhibited the most potent scavenging activities (**2**, **11**). After the compound **2** capturing the metal ions like Cu^{2+}, Fe^{3+} and Zn^{2+}, its

Table 1
DPPH scavenging activities and inhibitions of Aβ(1–42) self-induced aggregation of salphen derivatives.

Compounds	IC_{50} (μM)	Aβ(1–42) aggregation inhibition (%)[b]
	DPPH scavenging activities[a]	
1	233 ± 5.1	52.2 ± 2.6
2	21 ± 2.0	70.3 ± 2.1
3	144 ± 3.4	66.4 ± 1.0
4	135 ± 0.8	70.4 ± 1.7
5	338 ± 1.4	65.0 ± 0.8
6	483 ± 1.8	73.1 ± 1.6
7	322 ± 2.5	54.6 ± 0.9
8	>2000	33.7 ± 1.4
9	260 ± 7.7	35.8 ± 2.1
10	233 ± 4.0	42.9 ± 2.8
11	19 ± 1.3	59.0 ± 1.6
12	563 ± 5.7	57.8 ± 2.0
13	241 ± 4.4	69.9 ± 1.1
14	169 ± 3.0	65.5 ± 1.5
15	356 ± 2.8	27.4 ± 2.3
16	296 ± 3.6	65.5 ± 1.2
17	>2000	62.1 ± 1.7
18	17 ± 0.8	71.8 ± 2.2
19	193 ± 5.9	25.5 ± 0.9
20	727 ± 7.4	33.5 ± 1.6
21	483 ± 4.6	64.7 ± 0.9
22	27 ± 2.1	69.6 ± 1.7
23	16 ± 1.5	67.5 ± 2.2
24	130 ± 3.9	60.4 ± 1.1
25	147 ± 4.3	42.6 ± 2.0
26	398 ± 1.5	37.0 ± 1.3
Resveratrol[c]	109.4 ± 3.8	63.7 ± 2.3
Curcumin[c]	–	56.9 ± 1.7

[a] IC_{50} values were expressed as mean ± SD for three determinations.
[b] Inhibition of Aβ(1–42) self-induced aggregation, the thioflavin-T fluorescence method was used, the mean ± SD of at least three independent experiments and the measurements were carried out in the presence of 20 μM compounds.
[c] Resveratrol and curcumin were used as positive control.

metal complexes (**18**, **22**, **23**) could retain almost the same scavenging activities. In compounds **2**, **11**, **18**, **22**, **23** especially the combination of two OH group substitutions at the 2,5 positions of ring B is correlated with the highest scavenging response. The simultaneous presence of the two *para*-position OH groups enhances activities. A number of two OH group substitutions at the 2,4 positions of ring B derivatives showed reduced activities (**3**, **10**, **14**, **16**, **17**, **21**, **24**, **25**). Replacement of the 5-hydroxyl group on ring B by a chlorine group was found to reduce the ability of scavenging the DPPH free radical (**5**, **8** and **15**). This observation indicated that the chlorine group was negative for the activity compared to the hydroxyl group. IC_{50} values of compounds **8**–**15**, **17**, **21** and **25** indicated that no matter whether a CO_2CH_3 group or Cl atom on ring A was contributed relatively less to the DPPH-scavenging. Among the target compounds, compounds **2**, **11**, **18**, **22** and **23** (IC_{50} = 21.0, 19.0, 17.0, 27.0 and 16.0 μM) showed the most potent scavenging activity, which was 5.2, 5.7, 6.4, 4.0 and 6.8 times stronger than that of the reference compound resveratrol (IC_{50} = 109.4 μM).

2.3. In vitro antioxidant activity assays

Some compounds tested for their DPPH radical scavenging activities were also tested for their antioxidant activities by using the ABTS (2, 2′-azino-bis (3-ethylbenzthiazoline-6-sulfonicacid)) radical scavenging method [37]. Trolox, a water-soluble vitamin E analog, was used as a reference standard. Their antioxidant activities were provided as a trolox equivalent, with their relative potency at 25 μM compared with trolox. As shown in Fig. 2, compounds **2**, **4**, **11**, **18**, **22**, **23** had the ability to scavenge the ABTS radical with 2.6, 1.6, 1.8, 1.7, 0.8, 2.0 trolox equivalents respectively. All of these selected compounds demonstrated good antioxidant activities ranging from 0.8- to 2.6-fold of the trolox value. The best activity was observed for compounds bearing two *para*-position OH groups on the ring B. After the compound **2** captured the metal ions like Cu^{2+}, Fe^{3+} and Zn^{2+}, its metal complexes (**18**, **22**, **23**) showed decreased scavenging activities.

2.4. Inhibition of Aβ (1–42) self-induced aggregation

All compounds tested for their DPPH radical scavenging activities were also tested for their ability to inhibit Aβ (1–42) self-induced aggregation by using a thioflavin-T based fluorometric assay [38]. Curcumin (Cur) and resveratrol (Res) were used as reference compounds and the results are summarized in Table 1 and shown in Fig. 3. From the results, it could be seen that most compounds exhibited moderate-to-good potencies (25.5–73.1 % at 20 μM) compared to those of curcumin (56.9% at 20 μM) and resveratrol (63.7% at 20 μM). Noticeably, the optimal Aβ (1–42) aggregation inhibition potency (73.1% at 20 μM) was provided by compound **6**. Compounds **2**, **18**, **22**, **23** which exhibited the most potent radical-scavenging activity, had good Aβ aggregation inhibition property (70.3%, 71.8%, 69.6% and 67.5% at 20 μM). From the inhibition values of compounds **2**–**3**, **10**–**11**, **16**–**18** and **21**–**24**, it appeared that introduction of hydroxy groups into ring B seemed to be beneficial to Aβ self-induced aggregation inhibitory activity. With the exception of compounds **17** and **21**, the reduced activities were observed for compounds (**8**, **9**, **10**, **11**) bearing CO_2CH_3 on the ring A. According to the inhibition values of the metal compounds **16**–**26**, the different kinds of metal irons did not seem to play a role since the capturing compound **2** on Cu^{2+}, Fe^{3+} and Zn^{2+} respectively (**18**, **22** and **23**) did not influence dramatically the outcome of the experiments.

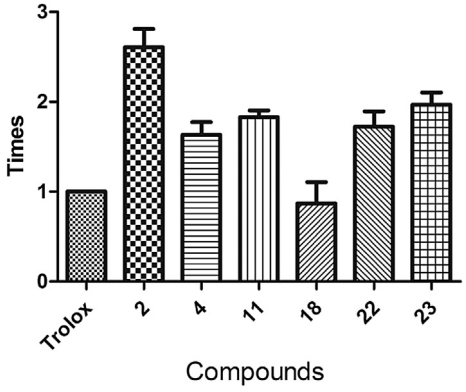

Fig. 2. The ABTS radical scavenging activities of salphen derivatives and their metal complexes. Trolox, a water-soluble vitamin E analog, was used as a reference standard (1.0 equiv).

2.5. Docking study of compound 2 with Aβ(1–42)

To further study the interaction mode of compound **2** for Aβ, molecular docking study was performed using software package MOE 2008.10. The X-ray crystal structure of the protein Aβ(1–42) structure (PDB code 1IYT) [39] used in the docking study was obtained from the Protein Data Bank. As shown in Fig. 4, ring B of compound **2** interacted with the Ser8 via π–π stacking interaction with the distance of 4.51 Å. A hydrogen bond interaction were found between ring B of compound **2** and His6, Arg5 residues with the distance of 4.32 and 3.76 Å, respectively. These results indicated that the hydrogen bond interactions played important roles in the stability of the **2**/Aβ (1–42) complex.

2.6. Metal chelating effect

The chelating effect of all compounds for metals such as Cu^{2+} and Fe^{2+} in methanol was studied by UV–vis spectrometry with wavelength ranging from 200 to 500 nm [40,41]. In Fig. 5(a), UV–vis spectra of compound **2** at increasing Cu^{2+} concentrations were shown as an example. The increase in absorbance, which could be better estimated by an inspection of the differential spectra (Fig. 5(b)), indicated that there was an interaction between Cu^{2+} and compound **2**. Similar behavior was also observed when using Fe^{2+}. These observations indicated that our compounds could effectively chelate Cu^{2+} and Fe^{2+}, and thereby could serve as metal chelators in treating AD. The ratio of ligand/metal ion in the complex was investigated by mixing the fixed amount metal ion with increasing ligand; it was possible to observe that the maximum intensity of difference spectra was reach at about 1:1 ratio, which was taken as an indication of the stoichiometry of the complex.

2.7. Inhibition of Cu^{2+}-induced Aβ(1–42) aggregation

To investigate the ability of the salphen derivatives to inhibit Cu^{2+}-induced Aβ (1–42) aggregation, we studied compounds **2**, **4** and **11** by a ThT-binding assay [42]. Resveratrol and clioquinol were used as reference compounds. It could be seen from Fig. 6, the fluorescence of Aβ treated with Cu^{2+} is 146.7% that of Aβ alone, which indicates that Cu^{2+} accelerates Aβ aggregation. By contrast, the fluorescence of Aβ treated with Cu^{2+} and the tested compounds decreased dramatically (**2**, 85.7% inhibition of Cu^{2+}-induced Aβ aggregation; **4**, 72.4% inhibition; **11**, 77.1% inhibition; CQ, 65.7% inhibition; Res, 60.4% inhibition). These results suggested that our compounds could inhibit Cu^{2+}-induced Aβ aggregation effectively by chelating Cu^{2+}.

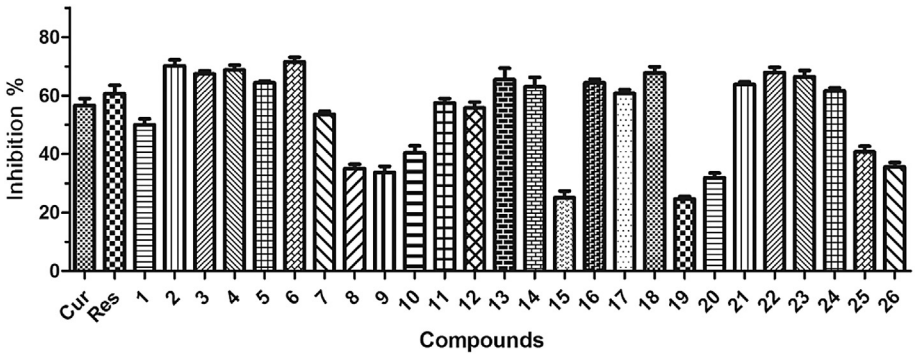

Fig. 3. Inhibition of Aβ (1–42) self-induced aggregation by compounds (**1**–**26**) comparing with those of curcumin (Cur) and resveratrol (Res). The thioflavin-T fluorescence method was used and the measurements were carried out in the presence of 20 μM test compound. The mean ± SD values from three independent experiments were shown.

2.8. Control of Cu^{2+}-Aβ H_2O_2 production by compound **2**

Binding of redox active metal ions such as Cu^{2+} to Aβ species is known to be involved in generation of ROS such as H_2O_2 and subsequent facilitation of Aβ aggregation and neurotoxicity. The effect of compound **2** on H_2O_2 production by Cu^{2+}–Aβ_{42} species was examined using the HRP/Amplex Red assay [43]. Under reducing conditions, the Cu^{2+}–Aβ (1–42) react with O_2 to generate H_2O_2. Addition of compound **2** to such a solution reduced the production of H_2O_2 by about 81% for the Cu^{2+}–Aβ (1–42) species. By comparison, the strong chelator ethylenediaminetetraacetic acid (EDTA) showed an even more pronounced effect, almost complete eliminating (>89%), and clioquinol (CQ) showed the reducing effect by about 74%. These results showed that compound **2** was able to chelate metal ions as well as regulated ROS production, which showed promise for their further applications (Fig. 7).

2.9. Cell viability and neuroprotection studies

To gain insight into the therapeutic potential of these derivatives, cell viability and neuroprotective capacity against oxidative stress were assayed using the human neuroblastoma cell line SH-SY5Y [44]. Compounds **2**, **4**, **11**, **18**, **22** and **23** were selected as representative compounds of different types. First, the colorimetric MTT [3-(4,5-dimethyl-2-thiazolyl)-2,5-diphenyl-2H-tetrazolium bromide] assay was performed to examine the potential cytotoxic effects of compounds **2**, **4**, **11**, **18**, **22** and **23**. As indicated in Fig. 8, compounds **2**, **4**, **11**, **18**, **22** and **23** did not show significant effect on cell viability at 1–50 μM after incubation for 24 h. This suggested that compounds **2**, **4** and **11** were nontoxicity to SH-SY5Y cells, and after the compound **2** capturing the metal ions like Cu^{2+}, Fe^{3+} and Zn^{2+}, its metal complexes (**18**, **22**, **23**) also showed nontoxicity to SH-SY5Y cells.

Compounds **2**, **11**, **18** and **23** were tested for their capacity to protect human SH-SY5Y neuroblastoma cells against oxidative stress-associated death induced by H_2O_2. Trolox and resveratrol were also used as the reference compounds. In this assay, addition of 200 μM H_2O_2 to the growth medium reduced cell viability to 65.7% compared to control. The tested compounds were added to the media at different concentrations immediately prior to the H_2O_2 insult. As can be seen in Fig. 9, all of the compounds exhibited neuroprotective effects at concentrations ranging from 1.25 to

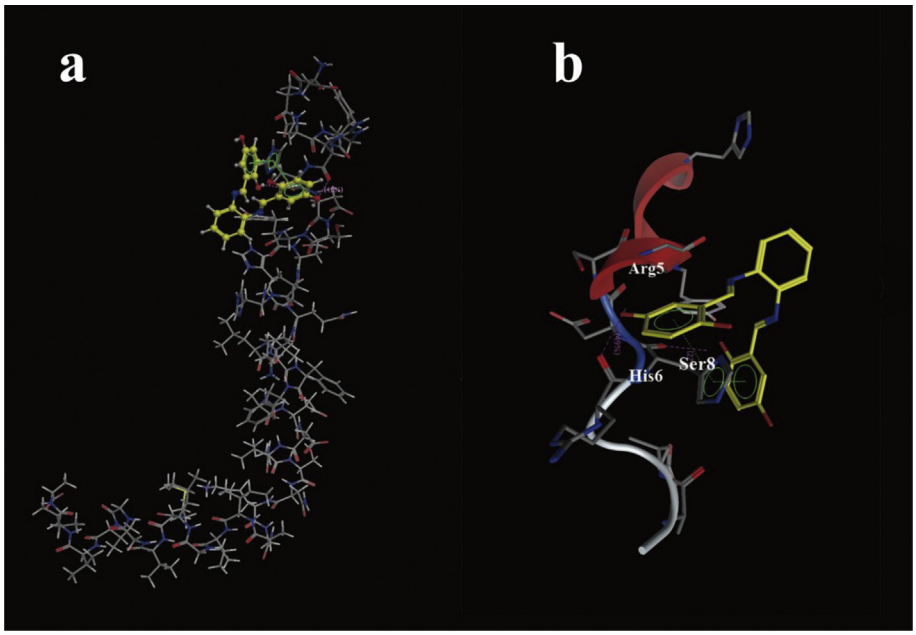

Fig. 4. Docking study of compound **2** (colored yellow) with Aβ (1–42) (PDB code 1IYT). (a) Cartoon representations of compound **2** interacting with Aβ (1–42). (b) Association of compound **2** (colored yellow) and the Aβ (1–42) obtained from docking calculations. The interactions between the ligand and residue Ser8 and His6 are indicated by the green line. (For interpretation of the references to color in this figure legend, the reader is referred to the web version of this article.

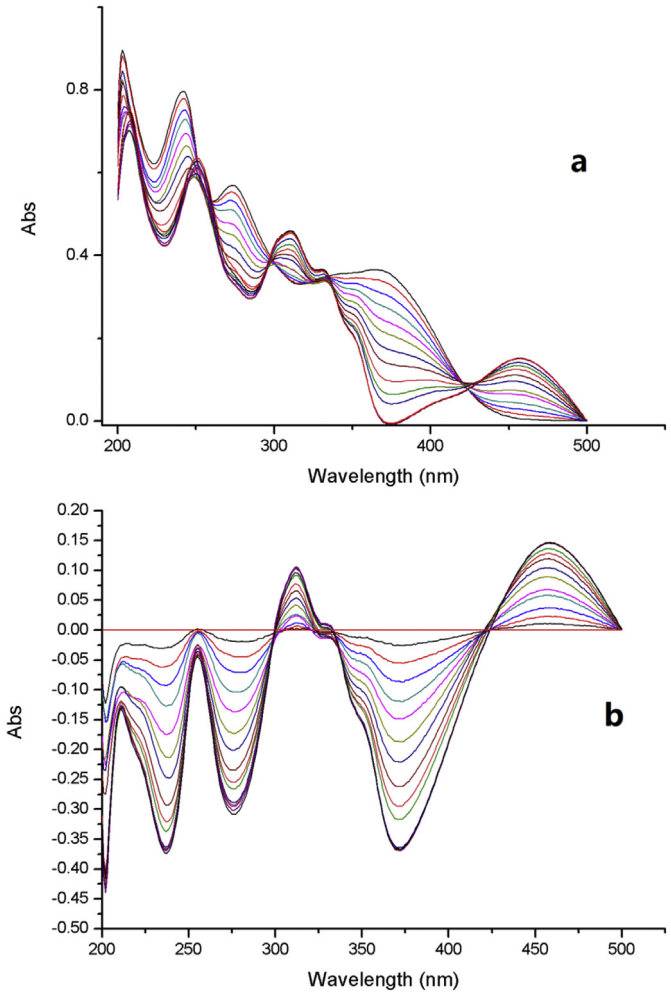

Fig. 5. (a) Uv–vis (200–500 nm) absorption spectra of compound **2** (25 μM) in methanol after addition of ascending amounts of $CuCl_2$ (2–50 μmol/L). (b) The differential spectra due to **2**-Cu^{2+} complex formation obtained by numerical subtraction from the above spectra of those of Cu^{2+} and **2** at the corresponding concentrations.

10 μM. Compounds **2**, **11** and metal complex **23** had showed the highest protective capability almost the same as trolox at the concentration of 10 μM and much better than resveratrol. The metal complex **18** showed moderate protective capabilities similar to resveratrol at the concentration of 10 μM. These observations further indicated that these new derivatives had the potential to be efficient multifunctional agents, including antioxidant activity, for the treatment of AD.

2.10. In vitro blood–brain barrier permeation assay

In the central nervous system (CNS) drug development, it is important that the compounds are able to cross the blood–brain barrier (BBB). So BBB permeability properties of CNS drug candidates should be determined as early as possible in the drug discovery process. To evaluate the potential for these compounds to cross the blood–brain barrier (BBB), we used a parallel artificial membrane permeation assay for BBB (PAMPA-BBB), which was described by Di et al. [45,47]. Assay validation was made by comparing experimental permeability of 9 commercial drugs with reported values (Table 2). A plot of experimental data versus bibliographic values gave a good linear correlation, P_e (exp.) = 0.8964 P_e (bibl.) − 0.1126 (R^2 = 0.9578) (Fig. 10). From this

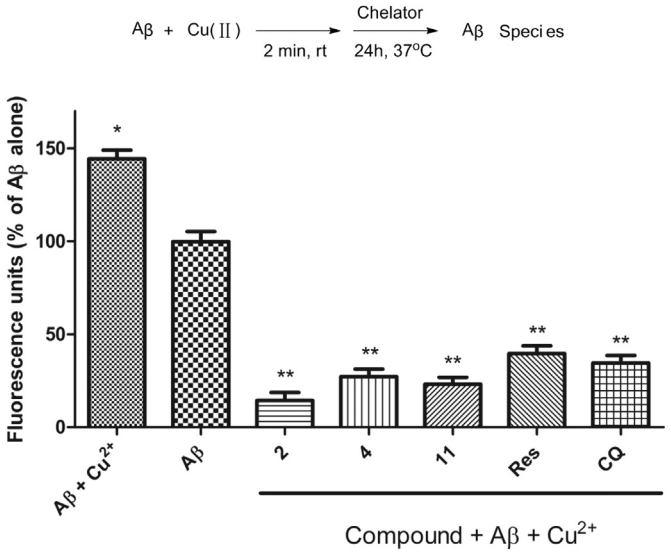

Fig. 6. Inhibition of Cu^{2+}-induced Aβ (1–42) aggregation by compounds **2**, **4** and **11** comparing with those of resveratrol (Res) and clioquinol (CQ) ([Aβ = 25 μM, [**2**] = 50 μM, [**4**] = 50 μM, [**11**] = 50 μM, [Res] = 50 μM, [CQ] = 50 μM, [Cu^{2+}] = 25 μM, 37 °C, 24 h). Values are reported as the mean ± SD of three independent experiments. $^{*}p < 0.05$, $^{**}p < 0.01$.

equation and taking into account the limit established by Di et al. for blood–brain barrier permeation, we classified compounds as follows:

(a) 'CNS +' (high BBB permeation predicted); P_e (10^{-6} cm s^{-1}) > 3.5.
(b) 'CNS −' (low BBB permeation predicted); P_e (10^{-6} cm s^{-1}) < 1.7.
(c) 'CNS +/−' (BBB permeation uncertain); P_e (10^{-6} cm s^{-1}) from 3.5 to 1.7.

The P_e values of these selected compounds are summarized in Table 2. From Table 2, it can be seen that compounds **2**, **18**, **22** and **23** are able to cross the blood–brain barrier (BBB).

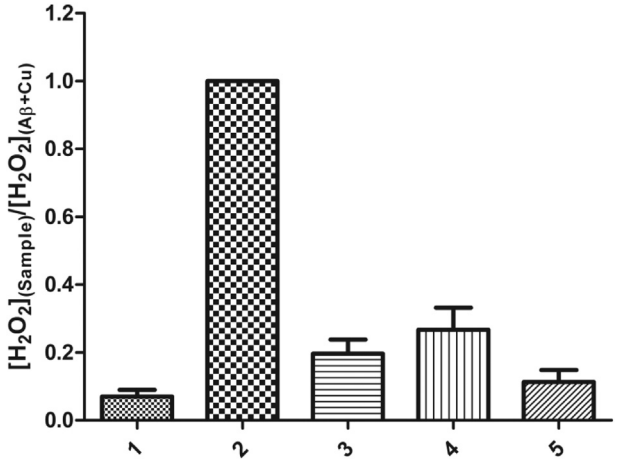

Fig. 7. Production of H_2O_2 from reactions of Aβ, Cu^{2+}, and compound upon addition of ascorbate, as determined by an HRP/Amplex-Red assay. Lanes: (1) Aβ; (2) Aβ + Cu^{2+}; (3) Aβ + Cu^{2+} + **2**; (4) Aβ + Cu^{2+} + CQ; (5) Aβ + Cu^{2+} + EDTA ([Aβ] = 200 nM, [Cu^{2+}] = 400 nM, [chelator] = 800 nM, [ascorbate] = 10 μM, [Amplex Red] = 50 nM, [HRP] = 0.1 U/mL, and $\lambda_{ex/em}$ = 530/590 nm). Values are reported as the mean ± SD of three independent experiments.

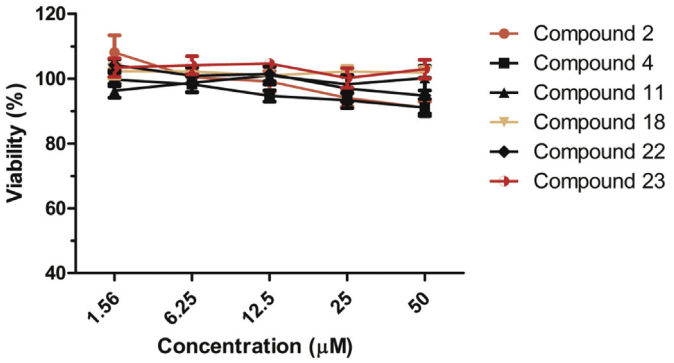

Fig. 8. Effects of compounds on cell viability in SH-SY5Y cells. The cell viability was determined by the MTT assay after 24 h of incubation with various concentrations of **2**, **4**, **11**, **18**, **22** and **23**. The results were expressed as a percentage of control cells. Values are reported as the mean ± SD of three independent experiments.

3. Conclusion

In conclusion, a series of salphen derivatives were designed and synthesized as multi-functional agents for the treatment of AD. Among the synthesized compounds, compound **2** exhibited significant inhibition of self-induced and Cu^{2+}-induced Aβ aggregation, antioxidant activity, metal-chelating ability, control of Cu^{2+}–Aβ H_2O_2 production and low cell toxicity. Furthermore, compound **2** showed neuroprotective capability much better than resveratrol at the concentration of 10 μM, and it was able to cross the blood–brain barrier. In addition, compound **2** retained the activities of antioxidant, anti Aβ aggregation and neuroprotection after capturing the metal ions Cu^{2+}, Fe^{3+} and Zn^{2+} (its metal complexes **18**, **22** and **23**). These properties highlighted that the compound **2** could serve as a new multifunctional drug candidate in the treatment of Alzheimer's disease.

4. Experimental section

4.1. Chemistry

All chemicals (reagent grade) used were purchased from Sinopharm Chemical Reagent Co., Ltd. (China). Reaction progress was monitored using analytical thin layer chromatography (TLC) on precoated silica gel GF_{254} (Qingdao Haiyang Chemical Plant, Qingdao, China) plates and the spots were detected under UV light (254 nm). Melting point was measured on an XT-4 micromelting point instrument and uncorrected. IR (KBr-disc) spectra were recorded by Bruker Tensor 27 spectrometer. ^{1}H NMR and ^{13}C NMR spectra were measured on a Bruker ACF-500 spectrometer at 25 °C and referenced to TMS. Chemical shifts were reported in ppm (δ) using the residual solvent line as internal standard. Splitting patterns were designed as s, singlet; d, doublet; t, triplet; m, multiplet. Mass spectra were obtained on an MS Agilent 1100 Series LC/MSD Trap mass spectrometer (ESI-MS). Elemental analyses were carried out on PerkinElmer 2400 Series II CHNS/O System, College of Pharmacy, China Pharmaceutical University, Nanjing, China.

Table 2
Permeability (P_e, 10^{-6} cm s^{-1}) in the PAMPA-BBB assay for 9 commercial drugs (Used in the Experiment Validation) and selected salphen derivatives.[a]

Compounds	Bibl.[b]	P_e (10^{-6} cm s^{-1})	Compounds	P_e (10^{-6} cm s^{-1})
Testosterone	17.0	15.0	**2**	5.7
Clonidine	5.3	5.2	**4**	2.9
Hydrocortisone	1.9	0.82	**11**	2.7
Corticosterone	5.1	3.21	**18**	9.5
Verapamil	16.0	10.08	**22**	5.7
β-Estradiol	12.0	13.2	**23**	3.6
Progesterone	9.3	6.7	–	–
Piroxicam	2.5	1.6	–	–
Dopamine	0.2	0.3	–	–

[a] Experimental data are the mean ± SD of 3 independent experiments, using PBS:EtOH (70:30) as solvent.
[b] Data from Ref. [46].

4.1.1. General procedures for the preparation of compounds ***1–26***

Two equivalents of the respective salicylaldehyde derivatives (7.0 mmol) in ethanol (20 mL) were added dropwise to a solution of one equivalent of 1,2-phenylenediamine derivatives in ethanol (10 mL). The mixture was stirred under reflux for 1–5 h and then allowed to cool down to room temperature. The product was collected, washed with ethanol and dried (P_2O_5). The obtained ligand (0.6 mmol) was dissolved in ethanol (10 mL) and heated to reflux in the presence one equivalent of the respective $FeCl_3 \cdot 6H_2O$, $Cu(OAc)_2 \cdot H_2O$ and $Zn(OAc)_2 \cdot 2H_2O$ in ethanol (5 mL). After 1–6 h, the mixture was cooled to room temperature, the solid was filtered off, washed with ethanol and dried in vacuo.

*4.1.1.1. 2,2′-((1E,1′E)-(1,2-Phenylenebis(azanylylidene))bis(methanylylidene))diphenol (**1**).* Yield 60%, light yellow solid, m.p.

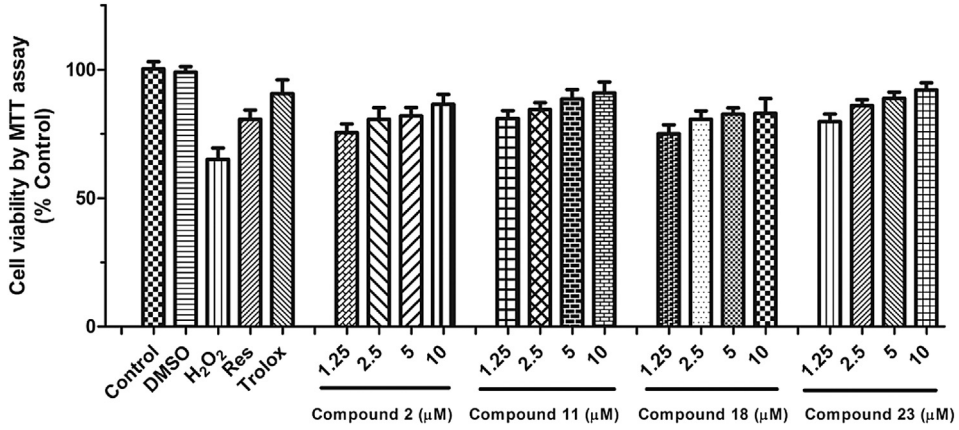

Fig. 9. Neuroprotection against H_2O_2 toxicity. Compounds **2**, **11**, **18** and **23** were tested for neuroprotective activity against H_2O_2 toxicity in SH-SY5Y neuroblastoma cell cultures. Resveratrol (10 μM) was used as the reference compound. Results are expressed as percent viability compared to cells not treated with H_2O_2. Data represent the mean ± SD of three observations. $^{***}p < 0.001$, $^{*}p < 0.05$, $^{**}p < 0.01$.

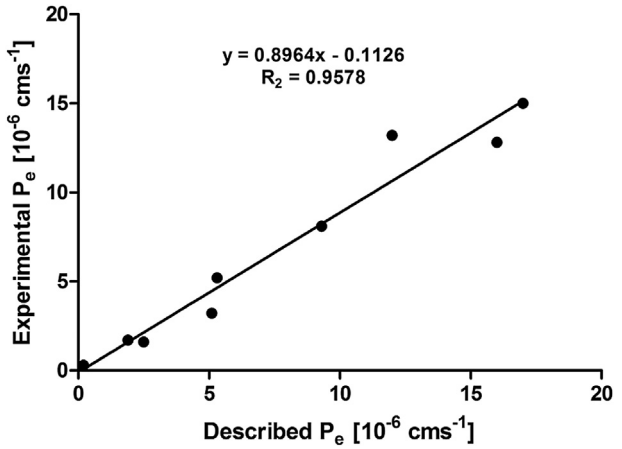

Fig. 10. Linear correlation between experimental and reported permeability of commercial drugs using the PAMPA-BBB assay.

167–168 °C, IR (KBr) ν 1614.02, 1561.94, 1480.45, 140.15, 1361.88, 1276.49, 1192.09, 1150.28, 1114.95, 909.96, 855.03, 830.60, 810.11, 787.25, 760.44, 639.92, 581.40, 510.45 cm^{-1}. ^1H NMR (500 MHz, DMSO) δ 12.96 (s, 2H), 8.95 (s, 2H), 7.71–7.67 (m, 2H), 7.48 (dd, J = 5.9, 3.5 Hz, 2H), 7.46–7.40 (m, 4H), 6.99 (t, J = 7.3 Hz, 4H). ^{13}C NMR (125 MHz, DMSO) δ 164.51, 160.89, 142.76, 133.90, 132.94, 128.26, 120.24, 119.99, 119.55, 117.16. ESI-MS m/z: 315.0 $[M-H]^-$.

*4.1.1.2. 2,2′-((1E,1′E)-(1,2-Phenylenebis(azanylylidene))bis(methanylylidene))bis (benzene-1,4-diol) (**2**).* Yield 64%, red solid, m.p. 226–227 °C, IR (KBr) ν 1619.64, 1572.10, 1483.32, 1352.75, 1299.69, 1209.68, 1156.74, 1047.41, 989.12, 885.24, 786.97, 747.04 cm^{-1}. ^1H NMR (500 MHz, DMSO) δ 12.14 (s, 2H), 9.09 (s, 2H), 8.80 (s, 2H), 7.41 (dd, J = 6.0, 3.4 Hz, 2H), 7.37 (dd, J = 5.8, 3.5 Hz, 2H), 7.04 (d, J = 2.9 Hz, 2H), 6.87 (dd, J = 8.8, 2.9 Hz, 2H), 6.79 (d, J = 8.8 Hz, 2H). ^{13}C NMR (125 MHz, DMSO) δ 164.16, 153.65, 149.98, 142.95, 127.92, 121.71, 120.24, 119.85, 117.61, 117.30. ESI-MS m/z: 383.0 $[M-H]^-$.

*4.1.1.3. 4,4′-((1E,1′E)-(1,2-Phenylenebis(azanylylidene))bis(methanylylidene))bis (benzene-1,3-diol) (**3**).* Yield 71%, yellow solid, m.p. >250 °C, IR (KBr) ν 1611.46, 1576.70, 1501.78, 1357.02, 1307.97, 1233.54, 1209.09, 1183.33, 1153.96, 1123.85, 847.27, 745.15, 532.22 cm^{-1} ^1H NMR (500 MHz, DMSO) δ 13.39 (s, 2H), 10.27 (s, 2H), 8.74 (s, 2H), 7.43 (d, J = 8.5 Hz, 2H), 7.37 (dt, J = 7.1, 3.6 Hz, 2H), 7.34–7.29 (m, 2H), 6.40 (dd, J = 8.5, 2.3 Hz, 2H), 6.30 (d, J = 2.2 Hz, 2H). ^{13}C NMR (125 MHz, DMSO) δ 163.72, 163.26, 163.04, 142.44, 134.77, 127.37, 119.89, 112.70, 108.23, 102.83. ESI-MS m/z: 347.0 $[M-H]^-$.

*4.1.1.4. 6,6′-((1E,1′E)-(1,2-Phenylenebis(azanylylidene))bis(methanylylidene))bis (2-methoxyphenol) (**4**).* Yield 55%, red solid, m.p. 172 °C, IR (KBr) ν 1612.74, 1573.95, 1467.09, 1400.89, 1256.55, 1205.60, 1077.70, 972.29, 781.06, 736.66 cm^{-1}. ^1H NMR (500 MHz, DMSO) δ 12.99 (s, 2H), 8.91 (s, 2H), 7.45 (dt, J = 7.1, 3.6 Hz, 2H), 7.42–7.37 (m, 2H), 7.25 (dd, J = 7.9, 1.4 Hz, 2H), 7.12 (dd, J = 8.0, 1.2 Hz, 2H), 6.90 (t, J = 7.9 Hz, 2H), 3.81 (s, 6H). ^{13}C NMR (125 MHz, DMSO) δ 164.63, 151.08, 148.31, 142.50, 128.14, 124.19, 120.19, 119.79, 118.91, 115.98, 56.14. ESI-MS m/z: 375.0 $[M-H]^-$.

*4.1.1.5. 2,2′-((1E,1′E)-(1,2-Phenylenebis(azanylylidene))bis(methanylylidene))bis (4-chlorophenol) (**5**).* Yield 67%, red solid, m.p. 213–214 °C, IR (KBr) ν 1614.36, 1565.17, 1475.69, 1384.97, 1350.11, 1273.84, 1189.43, 873.28, 845.21, 816.83, 790.39, 755.38, 716.03, 646.25, 499.33 cm^{-1}. ^1H NMR (500 MHz, DMSO) δ 12.90 (s, 2H), 8.94 (s, 2H), 7.79 (d, J = 2.7 Hz, 2H), 7.51–7.43 (m, 6H), 7.02 (d, J = 8.8 Hz, 2H). ^{13}C NMR (125 MHz, DMSO) δ 162.62, 159.44, 142.45, 133.26, 131.14, 128.47, 122.93, 121.24, 120.04, 119.12. ESI-MS m/z: 383.0 $[M-H]^-$.

*4.1.1.6. (N^1E,N^2E)-N^1,N^2-Bis(pyridin-2-ylmethylene)benzene-1,2-diamine (**6**).* Yield 63%, yellow solid, m.p. 212–213 °C, IR (KBr) ν 1646.84, 1583.64, 1464.84, 1438.48, 1388.72, 1312.21, 1209.00, 1151.13, 1114.34, 777.97, 724.04 cm^{-1}. ^1H NMR (500 MHz, $CDCl_3$) δ 8.96 (d, J = 8.5 Hz, 1H), 8.43 (d, J = 5.9 Hz, 1H), 8.39 (d, J = 4.8 Hz, 1H), 7.73–7.64 (m, 2H), 7.48 (d, J = 7.6 Hz, 1H), 7.41 (t, J = 7.4 Hz, 1H), 7.12–7.02 (m, 2H), 7.02–6.96 (m, 2H), 6.47 (d, J = 8.0 Hz, 1H), 5.22 (s, 2H). ^{13}C NMR (125 MHz, $CDCl_3$) δ 162.04, 154.75, 153.07, 148.75, 147.57, 141.28, 138.23, 137.59, 131.18, 131.11, 127.40, 126.00, 123.23, 118.55, 118.35, 116.59, 115.21. ESI-MS m/z: 287.0 $[M+H]^+$.

*4.1.1.7. 1,1′-((1E,1′E)-(1,2-Phenylenebis(azanylylidene))bis(methanylylidene))bis (naphthalen-2-ol) (**7**).* Yield 77%, yellow solid, m.p. 213 °C, IR (KBr) ν 1619.96, 1589.59, 1472.84, 1399.63, 1326.60, 1251.65, 1176.42, 968.39, 884.26, 820.45, 736.91 cm^{-1}. ^1H NMR (500 MHz, DMSO) δ 15.10 (d, J = 3.6 Hz, 2H), 9.69 (d, J = 3.5 Hz, 2H), 8.54 (d, J = 8.5 Hz, 2H), 7.96 (d, J = 9.2 Hz, 2H), 7.82 (d, J = 9.0 Hz, 4H), 7.55 (t, J = 7.6 Hz, 2H), 7.44 (dd, J = 6.0, 3.4 Hz, 2H), 7.37 (t, J = 7.4 Hz, 2H), 7.07 (d, J = 9.1 Hz, 2H). ^{13}C NMR (125 MHz, DMSO) δ 168.81, 157.83, 139.03, 137.09, 133.41, 129.35, 128.51, 127.75, 127.30, 123.98, 121.81, 121.00, 120.13, 109.68. ESI-MS m/z: 417.0 $[M+H]^+$.

*4.1.1.8. Methyl 3,4-bis((E)-(5-chloro-2-hydroxybenzylidene)amino) benzoate (**8**).* Yield 52%, light yellow solid, m.p. 192–194 °C, IR (KBr) ν 1717.50, 1618.36, 1562.63, 1477.18, 1434.95, 1356.21, 1307.72, 1279.16, 1182.21, 1120.24, 1190.11, 819.84, 762.84, 730.40, 649.06, 509.91 cm^{-1}. ^1H NMR (500 MHz, DMSO) δ 12.75 (s, 1H), 12.46 (s, 1H), 9.00 (s, 1H), 8.93 (s, 1H), 7.99 (d, J = 1.7 Hz, 1H), 7.96 (dd, J = 8.2, 1.8 Hz, 1H), 7.81 (d, J = 2.7 Hz, 1H), 7.80 (d, J = 2.7 Hz, 1H), 7.52 (d, J = 8.3 Hz, 1H), 7.45 (ddd, J = 10.3, 8.9, 2.7 Hz, 2H), 7.00 (t, J = 9.1 Hz, 2H), 3.90 (s, 3H). ^{13}C NMR (125 MHz, DMSO) δ 165.94, 163.38, 163.23, 159.45, 159.39, 146.98, 142.37, 133.77, 133.48, 131.21, 130.80, 129.06, 123.17, 123.02, 121.42, 121.28, 120.65, 120.58, 119.22, 119.14, 52.69. ESI-MS m/z: 441.0 $[M-H]^-$.

*4.1.1.9. Methyl 3,4-bis((E)-(2-hydroxy-3-methoxybenzylidene) amino)benzoate (**9**).* Yield 75%, yellow solid, m.p. 119–200 °C, IR (KBr) ν 1711.33, 1613.34, 1467.53, 1440.68, 1290.83, 1253.83, 1093.20, 971.74, 857.63, 769.10, 735.43 cm^{-1}. ^1H NMR (500 MHz, DMSO) δ 12.75 (s, 1H), 12.54 (s, 1H), 9.01 (s, 1H), 8.95 (s, 1H), 7.98–7.94 (m, 2H), 7.54 (d, J = 8.2 Hz, 1H), 7.30 (dd, J = 13.2, 7.3 Hz, 2H), 7.15 (t, J = 8.1 Hz, 2H), 6.92 (td, J = 7.9, 4.1 Hz, 2H), 3.90 (s, 3H), 3.82 (s, 3H), 3.81 (s, 3H). ^{13}C NMR (125 MHz, DMSO) δ 166.00, 165.58, 165.34, 151.11, 151.03, 148.37, 148.31, 146.86, 142.60, 128.86, 128.76, 124.22, 124.03, 120.77, 119.88, 119.86, 119.14, 119.02, 116.39, 116.22, 56.19, 56.12, 52.64. ESI-MS m/z: 435.0 $[M+H]^+$.

*4.1.1.10. Methyl 3,4-bis((E)-(2,4-dihydroxybenzylidene)amino)benzoate (**10**).* Yield 54%, light yellow solid, m.p. 233–234 °C, IR (KBr) ν 1716.44, 1625.55, 1584.17, 1490.33, 1436.50, 1399.19, 1716.44, 1625.55, 1584.17, 1490.38, 1436.50, 1399.19, 1283.58, 1266.09, 1216.45, 1127.61, 992.15, 877.03, 787.03, 763.45 cm^{-1}. ^1H NMR (500 MHz, DMSO) δ 11.92 (s, 1H), 11.73 (s, 1H), 9.11 (d, J = 12.6 Hz, 2H), 8.89 (s, 1H), 8.84 (s, 1H), 7.93 (d, J = 5.9 Hz, 2H), 7.49 (d, J = 8.7 Hz, 1H), 7.08 (dd, J = 8.3, 2.9 Hz, 2H), 6.89 (td, J = 8.5, 3.0 Hz, 2H), 6.79 (t, J = 8.2 Hz, 2H), 3.90 (s, 3H). ^{13}C NMR (125 MHz, DMSO) δ 166.07, 164.98, 164.76, 153.70, 153.65, 150.09, 150.91, 147.35, 143.02, 128.62, 128.52, 122.35, 122.02, 120.82, 120.78, 119.94, 119.90, 117.75, 117.64, 117.20, 116.93, 52.61. ESI-MS m/z: 405.0 $[M-H]^-$.

*4.1.1.11. Methyl 3,4-bis((E)-(2,5-dihydroxybenzylidene)amino)benzoate (**11**).* Yield 55%, yellow solid, m.p. >250 °C, IR (KBr) ν 1709.43, 1615.58, 1584.84, 1515.28, 1350.58, 1334.17, 1304.80, 1243.28, 1215.39, 1116.95, 986.29, 845.03, 766.39, 534.86 cm^{-1}. ^1H NMR (500 MHz, DMSO) δ 13.11 (d, J = 12.3 Hz, 2H), 10.32 (s, 2H), 8.83 (s, 1H), 8.80 (s, 1H), 7.91–7.86 (m, 2H), 7.52–7.45 (m, 3H), 6.41 (ddd, J = 8.5, 4.0, 2.3 Hz, 2H), 6.30 (t, J = 2.4 Hz, 2H), 3.88 (s, 3H). ^{13}C NMR (125 MHz, DMSO) δ 166.13, 164.20, 163.98, 163.91, 163.66, 163.62, 163.32, 146.73, 142.67, 134.98, 134.94, 128.12, 128.06, 120.52, 120.32, 112.72, 108.61, 108.40, 102.86, 102.81, 52.55. ESI-MS m/z: 407.0 $[M+H]^+$.

*4.1.1.12. 1,1′-((1E,1′E)-((4-Chloro-1,2-phenylene)bis(azanylylidene)) bis (methanylylidene))bis(naphthalen-2-ol) (**12**).* Yield 69%, yellow solid, m.p. 254–255 °C, IR (KBr) ν 1617.88, 1565.37, 1481.42, 1399.61, 1351.43, 1308.89, 1215.74, 1180.77, 969.46, 908.13, 818.54, 735.92, 470.94, 417.95 cm^{-1}. ^1H NMR (500 MHz, DMSO) δ 14.95 (d, J = 13.7 Hz, 2H), 9.70 (d, J = 13.0 Hz, 2H), 8.58 (dd, J = 10.1, 8.5 Hz, 2H), 8.07–7.92 (m, 3H), 7.83 (d, J = 8.4 Hz, 3H), 7.55 (t, J = 7.0 Hz, 2H), 7.46 (d, J = 10.5 Hz, 1H), 7.38 (t, J = 7.4 Hz, 2H), 7.07 (dd, J = 12.1, 9.2 Hz, 2H). ^{13}C NMR (125 MHz, DMSO) δ 168.85, 168.04, 158.60, 158.58, 140.33, 138.44, 137.43, 137.12, 133.40, 133.30, 131.88, 129.36, 129.34, 128.53, 127.41, 127.38, 127.13, 124.13, 124.08, 121.69, 121.46, 121.36, 121.15, 119.82, 109.86, 109.83. ESI-MS m/z: 451.0 $[M+H]^+$.

*4.1.1.13. 6,6′-((1E,1′E)-((4-Chloro-1,2-phenylene)bis(azanylylidene)) bis (methanylylidene))bis(2-methoxyphenol) (**13**).* Yield 77%, yellow solid, m.p. 215 °C, IR (KBr) ν 1614.07, 1464.74, 1408.09, 1253.03, 1207.52, 971.74, 780.18, 737.27 cm^{-1}. ^1H NMR (500 MHz, DMSO) δ 12.71 (d, J = 12.1 Hz, 2H), 8.96 (s, 1H), 8.92 (s, 1H), 7.59 (d, J = 1.8 Hz, 1H), 7.46 (dt, J = 8.5, 5.2 Hz, 2H), 7.29–7.23 (m, 2H), 7.14 (dd, J = 7.4, 4.1 Hz, 2H), 6.91 (td, J = 7.9, 3.9 Hz, 2H), 3.81 (s, 6H). ^{13}C NMR (125 MHz, DMSO) δ 165.63, 164.93, 151.03, 150.96, 148.31, 143.76, 141.60, 132.03, 127.58, 124.24, 124.10, 121.72, 120.06, 119.81, 119.77, 119.05, 119.02, 116.27, 116.14, 56.16. ESI-MS m/z: 409.0 $[M-H]^-$.

*4.1.1.14. 4,4′-((1E,1′E)-((4-Chloro-1,2-phenylene)bis(azanylylidene)) bis (methanylylidene))bis(benzene-1,3-diol) (**14**).* Yield 66%, yellow solid, m.p. >250 °C, IR (KBr) ν 1613.60, 1540.26, 1500.05, 1349.45, 1333.66, 1260.00, 1209.41, 1161.93, 1131.19, 982.09, 850.65, 805.52, 683.00, 520.33 cm^{-1}. ^1H NMR (500 MHz, Acetone) δ 13.21 (s, 1H), 13.12 (s, 1H), 9.19 (s, 2H), 8.77 (s, 1H), 8.73 (s, 1H), 7.41 (m, 4H), 7.33 (dd, J = 8.5, 2.2 Hz, 1H), 6.47 (ddd, J = 8.6, 6.7, 2.2 Hz, 2H), 6.38 (s, 2H). ^{13}C NMR (125 MHz, Acetone) δ 165.40, 164.84, 164.43, 164.37, 163.83, 163.66, 135.87, 135.65, 132.46, 127.43, 122.00, 120.59, 113.71, 113.66, 108.79, 108.70, 103.47. ESI-MS m/z: 383.0 $[M+H]^+$.

*4.1.1.15. 2,2′-((1E,1′E)-((4-Chloro-1,2-phenylene)bis(azanylylidene)) bis (methanylylidene))bis(4-chlorophenol) (**15**).* Yield 59%, yellow solid, m.p. 208–209 °C, IR (KBr) ν 1617.02, 1558.27, 1476.47, 1353.56, 1276.47, 1184.62, 1119.08, 1090.25, 930.58, 857.06, 836.75, 743.09, 658.81, 506.30 cm^{-1}. ^1H NMR (500 MHz, DMSO) δ 12.63 (d, 2H), 8.94 (s, 1H), 8.91 (s, 1H), 7.76 (s, 2H), 7.58 (d, J = 1.2 Hz, 1H), 7.51–7.41 (m, 4H), 7.00 (dd, J = 8.8, 3.5 Hz, 2H). ^{13}C NMR (125 MHz, DMSO) δ 163.48, 162.74, 159.37, 159.34, 143.75, 141.37, 133.56, 133.39, 132.35, 131.07, 130.99, 127.87, 123.05, 123.02, 121.50, 121.25, 121.21, 119.94, 119.14, 119.11. ESI-MS m/z: 419.0 $[M+H]^+$.

*4.1.1.16. N,N′-Bis-4-(hydroxysalicylidene)phenylenediamine–copper(II) (**16**).* Yield 74%, yellow solid, m.p. >250 °C; IR (KBr) ν 3442.44, 2921.08, 1605.96, 1555.87, 1452.04, 1369.86, 1237.45, 1206.12, 1117.78, 849.99, 792.24, 762.01, 646.76, 533.85, 495.30 cm^{-1}. Anal. Calcd for $C_{20}H_{14}CuN_2O_4$: C, 58.61; H, 3.44; N, 6.83. Found: C, 58.57; H, 3.39; N, 6.86. ESI-MS m/z: 408.0 $[M-H]^-$.

*4.1.1.17. N,N′-Bis-4-(hydroxysalicylidene)4-methylesterphenylenediamine–copper(II) (**17**).* Yield 63%, dark yellow solid, m.p. >250 °C; IR (KBr) ν 3451.21, 1697.04, 1619.07, 1531.49, 1442.61, 1370.86, 1336.01, 1238.66, 1194.26, 1139.01, 983.90, 842.88, 798.44, 762.01, 658.07, 636.64, 573.85, 538.85, 501.57, 474.88 cm^{-1}. Anal. Calcd for $C_{22}H_{16}CuN_2O_6$: C, 56.47; H, 3.45; N, 5.99. Found: C, 56.58; H, 3.51; N, 5.94. ESI-MS m/z: 466.0 $[M-H]^-$.

*4.1.1.18. N,N′-Bis-5-(hydroxysalicylidene)phenylenediamine–copper(II) (**18**).* Yield 56%, brown solid, m.p. >250 °C; IR (KBr) ν 3444.20, 1608.22, 1536.64, 1470.80, 1385.34, 1317.80, 1209.88, 1158.57, 967.05, 824.54, 748.44, 493.66, 438.02 cm^{-1}. Anal. Calcd for $C_{20}H_{14}CuN_2O_4$: C, 58.61; H, 3.44; N, 6.83. Found: C, 58.51; H, 3.48; N, 6.81. ESI-MS m/z: 408.0 $[M-H]^-$.

*4.1.1.19. N,N′-Bis-2-(hydroxynaphthaldehyde)phenylenediamine–copper(II) (**19**).* Yield 77%, yellow solid, m.p. >250 °C; IR (KBr) ν 3452.38, 2359.21, 1611.63, 1534.16, 1459.78, 1399.06, 1366.31, 1192.28, 831.15, 736.92, 655.57, 559.90, 495.59, 475.00 cm^{-1}. Anal. Calcd for $C_{28}H_{18}CuN_2O_2$: C, 70.36; H, 3.80; N, 5.86. Found: C, 70.31; H, 3.84; N, 5.75. ESI-MS m/z: 478.0 $[M+H]^+$.

*4.1.1.20. N,N′-Bis(salicylidene)phenylenediamine–iron(III) chloride (**20**).* Yield 45%, brown solid, m.p. >250 °C; IR (KBr) ν 3451.01, 1604.24, 1533.91, 1462.69, 1439.51, 1380.25, 1315.91, 1196.89, 1149.86, 1127.55, 923.77, 872.57, 812.96, 760.53, 615.16, 539.42, 493.12, 476.01, 428.77 cm^{-1}. Anal. Calcd for $C_{20}H_{14}ClFeN_2O_2$: C, 59.22; H, 3.48; N, 6.91. Found: C, 59.35; H, 3.31; N, 6.82. ESI-MS m/z: 406.0 $[M+H]^+$.

*4.1.1.21. N,N′-Bis-4-(hydroxysalicylidene)4-methylesterphenylenediamine–iron(III) chloride (**21**).* Yield 64%, brown solid, m.p. >250 °C; IR (KBr) ν 3388.82, 1706.19, 1611.62, 1579.40, 1538.80, 1439.67, 1378.25, 1242.90, 1208.59, 1136.27, 986.34, 853.14, 804.05, 766.01, 651.58, 635.19, 604.43, 533.06, 507.19, 463.15 cm^{-1}. Anal. Calcd for $C_{22}H_{16}ClFeN_2O_6$: C, 53.31; H, 3.25; N, 5.65. Found: C, 53.42; H, 3.24; N, 5.66. ESI-MS m/z: 494.0 $[M-H]^-$.

*4.1.1.22. N,N′-Bis-5-(hydroxysalicylidene)phenylenediamine–iron(III)chloride (**22**).* Yield 71%, black solid, m.p. >250 °C; IR (KBr) ν 3443.76, 1603.35, 1538.08, 1466.45, 1305.14, 1226.99, 1205.09, 1159.46, 967.91, 822.15, 754.32, 729.12, 687.88, 599.98, 539.51, 506.64, 476.06 cm^{-1}. Anal. Calcd for $C_{20}H_{14}ClFeN_2O_4$: C, 54.89; H, 3.22; N, 6.40. Found: C, 54.80; H, 3.26; N, 6.56. ESI-MS m/z: 436.0 $[M-H]^-$.

*4.1.1.23. N,N′-Bis-5-(hydroxysalicylidene)phenylenediamine–zinc(II) (**23**).* Yield 55%, yellow solid, m.p. >250 °C; IR (KBr) ν 3355.24, 1616.69, 1542.89, 1476.86, 1441.75, 1393.20, 1294.48, 1244.24, 1219.74, 1157.53, 965.83, 876.03, 858.26, 827.57, 806.73, 749.36, 599.09, 553.03, 486.90 cm^{-1}. ^1H NMR (500 MHz, DMSO) δ 8.89 (s, 2H), 8.49 (s, 2H), 7.88 (dd, J = 6.1, 3.5 Hz, 2H), 7.36 (dd, J = 6.1, 3.4 Hz, 2H), 6.86 (dd, J = 9.0, 3.2 Hz, 2H), 6.79 (d, J = 3.2 Hz, 2H), 6.61 (d, J = 9.0 Hz, 2H). ^{13}C NMR (125 MHz, DMSO) δ 167.38, 162.31, 145.15, 139.88, 127.45, 125.64, 123.94, 118.59, 118.43, 116.80. ESI-MS m/z: 411.0 $[M+H]^+$.

*4.1.1.24. N,N′-Bis-4-(hydroxysalicylidene)phenylenediamine–zinc(II) (**24**).* Yield 59%, yellow solid, m.p. >250 °C, IR (KBr) ν 3424.10, 1613.75, 1560.91, 1479.28, 1449.12, 1394.17, 1356.97, 1239.00, 1189.54, 1132.87, 990.86, 844.05, 792.41, 748.24, 653.87, 526.55, 487.22 cm^{-1}. ^1H NMR (500 MHz, DMSO) δ 9.75 (s, 2H), 8.82 (s, 2H), 7.78 (dd, J = 6.1, 3.5 Hz, 2H), 7.28 (dd, J = 6.1, 3.4 Hz, 2H), 7.23 (d, J = 9.1 Hz, 2H), 6.10–6.06 (m, 4H). ^{13}C NMR (125 MHz, DMSO)

δ 174.78, 164.13, 161.03, 139.89, 138.35, 126.50, 116.05, 114.30, 106.93, 105.15. ESI-MS *m/z*: 411.0 $[M+H]^+$.

*4.1.1.25. N,N′-Bis-4-(hydroxysalicylidene)-4-chlorophenylenediamine–zinc (II) (**25**).* Yield 79%, yellow solid, m.p. >250 °C, IR (KBr) ν 3407.85, 1619.26, 1547.46, 1476.18, 1450.11, 1389.76, 1362.30, 1220.00, 1178.54, 1130.47, 926.24, 843.57, 643.92, 535.81, 510.45, 420.76 cm^{-1}. ^1H NMR (500 MHz, DMSO) δ 9.83 (s, 2H), 8.86 (s, 1H), 8.82 (s, 1H), 7.90 (d, *J* = 1.6 Hz, 1H), 7.80 (d, *J* = 8.8 Hz, 1H), 7.32–7.20 (m, 3H), 6.09 (d, *J* = 8.7 Hz, 4H). ^{13}C NMR (125 MHz, DMSO) δ 175.20, 174.96, 164.57, 164.35, 161.93, 161.28, 141.15, 138.80, 138.63, 138.42, 130.87, 125.83, 117.68, 116.16, 114.30, 114.24, 106.88, 106.85, 105.54, 105.36. ESI-MS *m/z*: 445.0 $[M+H]^+$.

*4.1.1.26. N,N′-Bis-2-(hydroxynaphthaldehyde)phenylenediamine–zinc (II) (**26**).* Yield 66%, red solid, m.p. >250 °C, IR (KBr) ν 3450.17, 2346.92, 1612.30, 1577.48, 1534.96, 1459.81, 1431.24, 1399.16, 1362.66, 1185.44, 979.54, 827.60, 744.41, 661.71 cm^{-1}. ^1H NMR (500 MHz, DMSO) δ 9.83 (s, 2H), 8.46 (d, *J* = 8.5 Hz, 2H), 8.15 (dd, *J* = 6.1, 3.5 Hz, 2H), 7.82 (d, *J* = 9.2 Hz, 2H), 7.72 (d, *J* = 7.8 Hz, 2H), 7.53–7.47 (m, 2H), 7.41 (dd, *J* = 6.1, 3.3 Hz, 2H), 7.26 (t, *J* = 7.4 Hz, 2H), 7.02 (d, *J* = 9.2 Hz, 2H). ^{13}C NMR (125 MHz, DMSO) δ 174.05, 156.49, 140.62, 136.18, 136.00, 129.17, 127.88, 127.41, 127.07, 126.08, 122.10, 120.01, 117.13, 109.47. ESI-MS *m/z*: 479.0 $[M+H]^+$.

4.2. DPPH free radical-scavenging assay

DPPH was used to assess free radical-scavenging activity [36]. DPPH is one of the few stable and commercially available organic nitrogen radicals and has a UV–vis absorption maximum at 517 nm. Upon reduction, the solution color fades; the reaction progress is conveniently monitored by a spectrophotometer. To test free radical-scavenging effects, compounds **1**–**26** were adjusted with methanol solution to final concentrations of 0–200 μM. Methanolic DPPH (400 μM) was used in the reaction mixture. Serial dilutions of the test sample (20 μL) were combined with the DPPH (180 μL, 400 μM) solution in a 96-well microtitre plate. MeOH was used as a negative control and resveratrol was used as positive control. The reaction mixtures were incubated for 30 min at 37 °C in the dark and the change in absorbance at 517 nm was measured. Mean values were obtained from triplicate experiments. Inhibition percent was calculated using the equation: DPPH radical-scavenging rate (%) = $[1 - (A - C)/B] \times 100$, where *A* is the absorbance of the sample (DPPH + compounds), *B* is the absorbance of the DPPH radical-methanol solution, and *C* is the absorbance of the sample (compounds) alone. Percent inhibition was plotted against concentration, and the equation for the line was used to obtain the IC_{50} value. The IC_{50} values of samples were compared against the standard, resveratrol, and the lower the IC_{50} of synthesized compounds, the better it is as an antioxidant.

4.3. ABTS radical cation scavenging activity assay [46]

2, 2′-Azino-bis-2-ethybenz-thiazoline-6-sulfonic acid (ABTS) was dissolved in purified water to a 7 mM concentration. ABTS radical cation ($ABTS^+$) was produced by reacting ABTS stock solution with 2.45 mM potassium persulfate (final concentration) and allowing the mixture to stand in the dark at room temperature for at least 18 h before use. The stock solution of ABTS was serially diluted with sodium phosphate buffer (50 mM, pH 7.4) to 100 μM. Trolox, **2**, **4**, **11**, **18**, **22** and **23** at different concentrations (total volume of 50 μL) were added to 150 μL of 100 μM ABTS solution, respectively. After the addition of either trolox or another antioxidant to the ABTS solution, complete mixing of reactants was achieved by bubbling three to four times using plastic pipettes. The optical absorbance of ABTS at 415 nm was measured at 6 min after addition and equilibrated at 30 °C. Each individual treatment was repeated for three times and the results of the experiments were compared.

4.4. Inhibition of Aβ (1–42) self-induced aggregation

Inhibition of Aβ (1–42) aggregation was measured using a Thioflavin T (ThT)-binding assay [38]. HFIP pretreated Aβ (1–42) samples (Anaspec Inc) were resolubilized with a 50 mM phosphate buffer (pH 7.4) to give a 25 μM solution. Each tested compound was firstly prepared in DMSO at a concentration of 10 mM and 1 μL of each was added to the well of black, opaque Corning 96-well plates such that the final solvent concentration was 10%. The final concentration of each compound was 20 μM and was prepared in independent triplicates. The solvent control was also included. Then, 9 μL of 25 μM Aβ (1–42) sample was added to each well and the samples mixed by gentle trapping. Plates were covered to minimize evaporation and incubated in dark at room temperature for 46–48 h with no agitation. After the incubation period, 200 μL of 5 μM ThT in 50 mM glycine-NaOH buffer (pH 8.0) was added to each well. Fluorescence was measured on a SpectraMax M5 (Molecular Devices, Sunnyvale, CA, USA) multi-mode plate reader with excitation and emission wavelengths at 446 nm and 490 nm, respectively. The fluorescence intensities were compared and the percent inhibition due to the presence of the inhibitor was calculated by the following formula: $100 - (IF_i/IF_o \times 100)$ where IF_i and IF_o are the fluorescence intensities obtained for Aβ (1–42) in the presence and in the absence of inhibitor, respectively.

4.5. Docking study

Molecular modeling calculations and docking studies were performed using Molecular Operating Environment (MOE) software version 2008.10 (Chemical Computing Group, Montreal, Canada). The X-ray crystal structure of Aβ (1–42) (PDB 1IYT) used in the docking study was obtained from the Protein Data Bank (www.rcsb.org). Heteroatoms and water molecules in the PDB file were removed at the beginning, and all hydrogen atoms were added to the protein. Amber99 force field was assigned to the enzyme and the partial charges were calculated with the same force field. Protonate states of the enzyme at pH 7 were obtained by following the Protonate 3D protocol in which all configurations were set as default. Compound **2** was drawn in MOE with all hydrogen atoms added. During the docking procedure, pose of compound **2** was initially generated by Triangle Matcher method, and scored with london dG function. 30 Poses of the compound were dedicated to the next refinement procedure. All poses were fine tune with the force field refinement scheme. The best 10 poses of molecules were retained and scored. After docking, the geometry of resulting complex was studied using the MOE's pose viewer utility.

4.6. Spectrophotometric measurement of complex with Cu^{2+} and Fe^{2+}

The study of metal chelation was performed in methanol at 298 K using UV–vis spectrophotometer (SHIMADZU UV-2450PC) with wavelength ranging from 200 to 500 nm [40,41]. The difference UV–vis spectra due to complex formation was obtained by numerical subtraction of the spectra of the metal alone and the compound alone (at the same concentration used in the mixture) from the spectra of the mixture. A fixed amount of **2** (25 μmol/L) was mixed with growing amounts of copper ion (2–50 μmol/L) and tested the difference UV–vis spectra to investigate the ratio of ligand/metal in the complex.

4.7. Inhibition of Cu^{2+}-induced Aβ(1–42)aggregation

For the inhibition of Cu^{2+}-induced Aβ (1–42) aggregation experiment [42], the Aβ was diluted in 20 μM HEPES (pH 6.6) with 150 μM NaCl. The mixture of the peptide (10 μL, 25 μM, final concentration) with or without copper (10 μL, 25 μM, final concentration) and the test compound (10 μL, 50 μM, final concentration) was incubated at 37 °C for 24 h. The 20 μL of the sample was diluted to a final volume of 200 μL with 50 mM glycine-NaOH buffer (pH 8.0) containing thioflavin T (5 μM). The detection method was the same as that of self-induced Aβ aggregation experiment.

4.8. Hydrogen peroxide assays

Hydrogen peroxide production was determined using an HRP/Amplex Red assay. A general protocol from Invitrogen's Amplex Red Hydrogen Peroxide/Peroxidase Assay as followed [43]. Reagents were added directed to a 96-well plate in the following order to give a 100 μL final solution: $CuCl_2$ (400 nM), phosphate buffer, Aβ peptide (200 μM), compounds (800 nM, 1% v/v DMSO), sodium ascorbate (10 μM). The reaction was allowed to incubate for 30 min at room temperature. After this incubation, 50 μM of freshly prepared working solution containing 100 nM Amplex Red (Sigma) and 0.2 U/mL HRP (Sigma) in phosphate buffer was added to each well, and the reaction was allowed to incubate for 30 min at room temperature. Fluorescence was measured using a SpectraMax Paradigm plate reader ($\lambda_{ex}/\lambda_{em}$ = 530/590). Error bars represent standard deviations for at least three measurements.

4.9. Cell culture and MTT assay for cell viability

The SH-SY5Y cells were cultured in Eagle's minimum essential medium (EMEM)/ham's F-12 (1:1) medium supplemented with 10% fetal bovine serum (FBS), 100 U/mL penicillin and 100 μg/mL streptomycin, at 37 °C in a humidified atmosphere containing 5% CO_2. Cells were subcultured in 96-well plates at a seeding density of 1×10^4 cells/well and allowed to adhere and grow. When cells reached the required confluence, they were placed into serum-free medium and treated with compounds **2**, **4**, **11**, **18**, **22** and **23**. Twenty-four hours later the survival of cells was determined by MTT assay. Briefly, after incubation with 20 μL of MTT at 37 °C for 4 h, living cells containing MTT formazan crystals were solubilized in 200 μL DMSO. The absorbance of each well was measured using a microculture plate reader with a test wavelength of 570 nm and a reference wavelength of 630 nm. Results are expressed as the mean ± SD of three independent experiments.

4.10. Neuroprotection activity in SH-SY5Y cells

SH-SY5Y cells were seeded at 1×10^4 cells/well in 96-well plates. After 24 h, the medium was removed and replaced with the tested compounds (1.25, 2.5, 5, 10 μM) at 37 °C and incubated for another 24 h. Resveratrol and trolox were used as the control with concentrations of 10 μM. Then, the cells were exposed to H_2O_2 (100 μM) and incubated at 37 °C for 24°h before assayed with MTT [44]. Results are expressed as percent viability compared to untreated cells.

4.11. In vitro blood–brain barrier permeation assay [47,48]

Brain penetration of compounds was evaluated using a parallel artificial membrane permeation assay (PAMPA) in a similar manner as described by Di et al. Commercial drugs were purchased from Sigma and Alfa Aesar. The porcine brain lipid (PBL) was obtained from Avanti Polar Lipids. The donor microplate (PVDF membrane, pore size 0.45 mm) and the acceptor microplate were both from Millipore. The 96-well UV plate (COSTAR®) was from Corning Incorporated. The acceptor 96-well microplate was filled with 300 μL of PBS/EtOH (7:3), and the filter membrane was impregnated with 4 μL of PBL in dodecane (20 mg/mL). Compounds were dissolved in DMSO at 5 mg/mL and diluted 50-fold in PBS/EtOH (7:3) to achieve a concentration of 100 mg/mL, 200 μL of which was added to the donor wells. The acceptor filter plate was carefully placed on the donor plate to form a sandwich, which was left undisturbed for 16 h at 25 °C. After incubation, the donor plate was carefully removed and the concentration of compound in the acceptor wells was determined using a UV plate reader (Flexstation® 3). Every sample was analyzed at five wavelengths, in four wells, in at least three independent runs, and the results are given as the mean ± standard deviation. In each experiment, 9 quality control standards of known BBB permeability were included to validate the analysis set.

Acknowledgments

This research work was financially supported by Innovative Research Team in University (IRT1193), A Project Funded by the Priority Academic Program Development of Jiangsu Higher Education Institutions (PAPD), Project of Graduate Education Innovation of Jiangsu Province (No. CXZZ13_0320).

Appendix A. Supplementary data

Supplementary data related to this chapter can be found at http://dx.doi.org/10.1016/j.ejmech.2014.10.004. These data include MOL files and InChiKeys of the most important compounds described in this article.

References

[1] M. Goedert, M.G. Spillantini, Science 314 (2006) 777–781.
[2] W. Thies, L. Bleiler, Alzheimer's Dement. 9 (2013) 208–245.
[3] R.J. Perrin, A.M. Fagan, D.M. Holtzman, Nature 461 (2009) 916.
[4] F.M. LaFerla, K.N. Green, S. Oddo, Nat. Rev. Neurosci. 8 (2007) 499.
[5] R. Jakob-Roetne, H. Jacobsen, Angew. Chem. Int. Ed. 48 (2009) 3030–3059.
[6] M. Jucker, L.C. Walker, Ann. Neurol. 70 (2011) 532–540.
[7] C. Haass, D.J. Selkoe, Nat. Rev. Mol. Cell. Biol. 8 (2007) 101–112.
[8] J. Kaffy, D. Brinet, J.L. Soulier, L. Khemtémourian, O. Lequin, M. Taverna, B. Crousse, S. Ongeri, Eur. J. Med. Chem. 86 (2014) 752–758.
[9] Y.S. Kim, S.H. Jung, B.G. Park, M.K. Ko, H.S. Jang, K. Choi, J.H. Baik, J. Lee, J.K. Lee, A.N. Pae, Y.S. Cho, S.J. Min, Eur. J. Med. Chem. 62 (2013) 71–83.
[10] A. Rauk, Chem. Soc. Rev. 38 (2009) 2698–2715.
[11] F. Molina-Halogado, R.C. Hider, A. Gaeta, R. Williams, P. Francis, Biometals 20 (2007) 639.
[12] C.J. Maynard, A.I. Bush, C.L. Masters, R. Cappai, Q.-X. Li, Int. J. Exp. Pathol. 86 (2005) 147–159.
[13] D.G. Smith, R. Cappai, K.J. Barnham, Biochim. Biophys. Acta 1768 (2007) 1976–1990.
[14] P. Zatta, D. Drago, S. Bolognin, S.L. Sensi, Trends Pharmacol. Sci. 30 (2009) 346–355.
[15] C. Hureau, P. Faller, Biochimie 91 (2009) 1212–1217.
[16] D.J. Bonda, H.-G. Lee, J.A. Blair, X. Zhu, G. Perry, M.A. Smith, Metallomics 3 (2011) 267–270.
[17] K. Jomova, M. Valko, Toxicology 283 (2011) 65–87.
[18] A.S. DeToma, S. Salamekh, A. Ramamoorthy, M.H. Lim, Chem. Soc. Rev. 41 (2012) 608–621.
[19] X. Zhu, B. Su, X. Wang, M.A. Smith, G. Perry, Cell. Mol. Life Sci. 64 (2007) 2202–2210.
[20] J. Shearer, P.E. Callan, T. Tran, V.A. Szalai, Chem. Commun. 46 (2010) 9137–9139.
[21] L.E. Scott, C. Orvig, Chem. Rev. 109 (2009) 4885–4910.
[22] J.H. Jang, Y.J. Surh, Free Radic. Biol. Med. 34 (2003) 1100–1110.
[23] M. Narasimhulu, T. Srikanth Reddy, K. Chinni Mahesh, A. Sai Krishna, J. Venkateswara Rao, Y. Venkateswarlu, Bioorg. Med. Chem. Lett. 19 (2009) 3125–3127.
[24] W. Zhang, S. Oya, M.P. Kung, C. Hou, D.L. Maier, H.F. Kung, J. Med. Chem. 48 (2005) 5980–5988.
[25] I. Lee, Y.S. Choe, J.Y. Choi, K.H. Lee, B.T. Kim, J. Med. Chem. 55 (2012) 883–892.

[26] S.S. Hindo, A.M. Mancino, J.J. Braymer, Y. Liu, S. Vivekanandan, A. Ramamoorthy, M.H. Lim, J. Am. Chem. Soc. 131 (2009) 16663–16665.
[27] E.R. Vardy, I. Hussain, N.M. Hooper, Expert Rev. Neurother. 6 (2006) 695–704.
[28] J.S. Choi, J.J. Braymer, R.P. Nanga, A. Ramamoorthy, M.H. Lim, Proc. Natl. Acad. Sci. U. S. A. 107 (2010) 21990–21995.
[29] S.S. Xie, X.B. Wang, J.Y. Li, L. Yang, L.Y. Kong, Eur. J. Med. Chem. 64 (2013) 540–553.
[30] S.Y. Li, N. Jiang, S.S. Xie, X.B. Wang, L.Y. Kong, Org. Biomol. Chem. 12 (2014) 801–804.
[31] S.Y. Li, X.B. Wang, L.Y. Kong, Eur. J. Med. Chem. 71 (2014) 36–45.
[32] M. Orhan Püsküllü, B. Tekiner, S. Suzen, Mini Rev. Med. Chem. 13 (2013) 365–372.
[33] B.H. Havsteen, Pharmacol. Ther. 96 (2002) 67–202.
[34] C.A. Rice-Evans, N.J. Miller, G. Paganga, Free Radic. Biol. Med. 20 (1996) 933–956.
[35] A. Hille, I. Ott, A. Kitanovic, I. Kitanovic, H. Alborzinia, E. Lederer, S. Wölfl, N. Metzler-Nolte, S. Schäfer, W.S. Sheldrick, C. Bischof, U. Schatzschneider, R. Gust, J. Biol. Inorg. Chem. 14 (2009) 711–725.
[36] J.C. Jung, E. Lim, Y. Lee, J.M. Kang, H. Kim, S. Jang, S. Oh, M. Jung, Eur. J. Med. Chem. 44 (2009) 3166–3174.
[37] T. Herraiz, J. Galisteo, Free. Radic. Res. 36 (2002) 923–931.
[38] M. Bartolini, C. Bertucci, M.L. Bolognesi, A. Cavalli, C. Melchiorre, V. Andrisano, ChemBioChem 8 (2007) 2152–2161.
[39] C. Yang, X. Zhu, J. Li, R. Shi, J. Mol. Model. 16 (2010) 813–821.
[40] W. Huang, D. Lv, H. Yu, R. Sheng, S.C. Kim, P. Wu, K. Luo, J. Li, Y. Hu, Bioorg. Med. Chem. 18 (2010) 5610–5615.
[41] R. Joseph, B. Ramanujam, A. Acharya, A. Khutia, C.P. Rao, J. Org. Chem. 73 (2008) 5745–5758.
[42] C. Lu, Y. Guo, J. Yan, Z. Luo, H.B. Luo, M. Yan, L. Huang, X. Li, J. Med. Chem. 56 (2013) 5843–5859.
[43] R.A. Himes, G.Y. Park, G.S. Siluvai, N.J. Blackburn, K.D. Karlin, Angew. Chem. Int. Ed. Engl. 47 (2008) 9084–9087.
[44] H. Zheng, M.B. Youdim, M. Fridkin, J. Med. Chem. 52 (2009) 4095–4098.
[45] M.I. Fernández-Bachiller, C. Pérez, L. Monjas, J. Rademann, M.I. Rodríguez-Franco, J. Med. Chem. 55 (2012) 1303–1317.
[46] N.J. Miller, C.A. Rice-Evans, Free. Radic. Res. 26 (1997) 195.
[47] B.C. Magliaro, C.J. Saldanha, Brain Res. 14 (2009) 1283.
[48] L. Di, E.H. Kerns, K. Fan, O.J. McConnell, G.T. Carter, Eur. J. Med. Chem. 38 (2003) 223–232.